PROCEEDINGS OF SCIENCE

Review of Lattice Muon $g-2$ HLbL Calculation

Luchang Jin*
Physics Department, University of Connecticut, Storrs, Connecticut 06269-3046, USA
RIKEN BNL Research Center, Brookhaven National Laboratory, Upton, New York 11973, USA
E-mail: ljin.luchang@gmail.com

Recent lattice QCD results for hadron light-by-light scattering (HLbL) and its contribution to muon anomalous magnetic moments ($g-2$) will be reviewed. There are currently more than three standard deviations between the BNL experimental result and the theoretical prediction. The Fermilab/JPARC experiments will reduce the experimental uncertainty by a factor of four. The uncertainty of theory prediction needs to be reduced to a similar level. With the recent progress in the dispersive approaches and the lattice calculations in determining the hadron vacuum polarization (HVP) contribution to muon $g-2$, HLbL is becoming the leading source of uncertainty in the theoretical prediction. Lattice QCD provides a systematic improvable way to calculate HLbL and a result with reliable error can be eventually obtained. In this regard, I overview the recent progress in the lattice calculations of HLbL, the current status of the calculation, and the future plans. In particular, I would discuss the method for handling the finite volume errors and discretization errors.

The 36th Annual International Symposium on Lattice Field Theory - LATTICE2018
22-28 July, 2018
Michigan State University, East Lansing, Michigan, USA.

*Speaker.

PoS(LATTICE2018)012

1. Introduction

Muon anomalous magnetic moments is one of the most precisely measured physical observables. The dimensionless number, $a_\mu = (g-2)/2$, is defined through the following relation:

$$\vec{\mu} = 2(1+a_\mu)\frac{-e}{2m_\mu}\vec{s} \tag{1.1}$$

where $\vec{\mu}$ is the magnetic moment of muon and $\vec{s}$ is its spin. The value of a_μ can be calculated theoretically using quantum field theory through the photon-muon vertex function:

$$\bar{u}(p')[F_1(q^2)\gamma_\nu + iF_2(q^2)[\gamma_\nu,\gamma_\rho]q_\rho/(4m_\mu)]u(p), \tag{1.2}$$

and $a_\mu = F_2(q^2=0)$. The diagram for the photon-muon vertex is Fig. 1 left. At leading order, a_μ is given by the 1-loop diagram, Fig. 1 right.

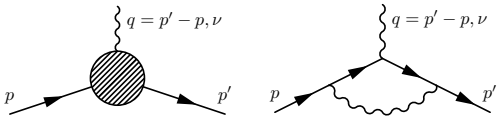

Figure 1: Left: photon-muon vertex. Right: leading contribution to muon anomalous magnetic moments, $a_\mu = \alpha/(2\pi) = 11614097.3242 \times 10^{-10}$ [1].

Table 1 shows the contribution to muon $g-2$ from different kinds of interactions. The most recent experimental value for muon $g-2$ is still given by BNL E821 [2]. The theoretical result has been calculated to very high precision. It turned out that the experimental result is larger than the standard model prediction by about three standard deviations. This deviation may be a definite signal of physics beyond the standard model. To exploit this chance to discover new physics, two new experimental efforts, the on-going Fermilab E989 [3] and the planned J-PARC E34 [4], are aiming at reducing the experimental uncertainty by a factor of four.

	$a_\mu \times 10^{10}$	
QED incl. 5-loops	11658471.8853 ± 0.0036	Aoyama, et al, 2012 [5]
Weak incl. 2-loops	15.36 ± 0.10	Gnendiger et al, 2013 [6]
HVP LO	692.5 ± 2.7	RBC-UKQCD and FJ17 combined [7, 8]
HVP NLO	-9.93 ± 0.07	FJ17 [8]
HVP NNLO	1.22 ± 0.01	FJ17 [8]
HLbL	10.3 ± 2.9	FJ17 [8]
Standard Model	11659181.3 ± 4.0	
Experiment (0.54 ppm)	11659208.9 ± 6.3	E821, The $g-2$ Collab. 2006 [2]
Difference (Exp $-$ SM)	27.6 ± 7.4	

Table 1: Standard model theory and current experiment comparison

In addition to the new experiments, we also need to further reduce the theoretical uncertainty of muon $g-2$ in order to fully profit from the expected, much more precise experimental $g-2$ results. It can be seen from Table 1 that the theoretical uncertainties are dominated by two hadronic processes, HVP LO and HLbL, shown in Fig. 2. The HVP LO value has been constantly improving due to efforts on the $e^+e^- \to$ hadrons experiment and analysis [8] and efforts on combining lattice with experimental data [7]. On the other hand, the present value for HLbL is still given by

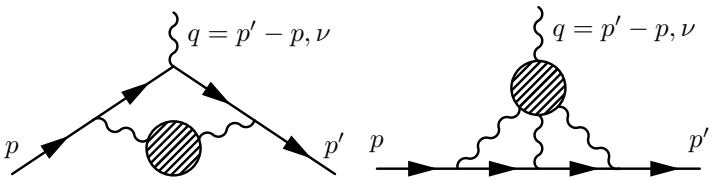

Figure 2: Left: hadronic vacuum polarization, leading order (HVP LO). Right: hadronic light-by-light (HLbL).

models [9, 8], whose uncertainty is less reliable. In Ref. [10], it is shown that many models for the charged pion loop contribution are not consistent with low-momentum behavior implied by quantum chromodynamics. In addition, it is hard to systematically improve the model results. In fact, its uncertainty has not changed much since the 2009 "Glasgow Consensus" [9], and is becoming the leading source of uncertainty in the theoretical prediction!

In additional to model calculation, there are efforts to develop dispersive relations for HLbL [11, 12, 13, 14]. The relations are more complicated and less effective compared with the dispersive relation for HVP, where all intermediate states contribute in the same form. For HLbL, different intermediate states appear in different integrals. For now, three channels have been analyzed, summarized in Table 2. The table, where contributions are classified by different processes, is similar to the model calculation. The difference is that each channel in the dispersive approach is well defined, and very accurately determined. For now, the explicit form of the dispersive integrals has been derived for up to two-particle intermediate states, but some measurable quantities that enter these integrals (e.g. the $\gamma^*\gamma^* \to \pi\pi$ helicity amplitudes) have not yet been measured other than in corners of the phase space [15].

	$a_\mu \times 10^{10}$	
π^0-pole	6.26(28)	[12]
π-box	$-1.59(2)$	[13, 14]
$\pi\pi$, π-pole LHC	$-0.8(1)$	[13, 14]

Table 2: Dispersive analysis of HLbL. Three channels have been analyzed.

Another systematically improvable method to calculate the HLbL diagram (Fig. 2 right) is lattice QCD. The quantity a_μ^{HLbL}, in general, can be expressed in the following form in Euclidean space:

$$\begin{aligned} a_\mu^{\mathrm{HLbL}} &= F_2^{\mathrm{HLbL}}(q^2 = 0) \\ &= \text{some factors} \otimes \text{Hadronic 4-point function } (\mathscr{H}) \otimes \text{Muon line function with photons } (\mathscr{M}). \end{aligned} \tag{1.3}$$

The non-perturbative hadronic 4-point function $\mathscr{H}$ should be obtained via lattice calculation. The 4-point function involves several diagrams, shown in Fig. 3. Not that we only draw the quark loops which are directly connected to the photons. These quark loops require explicit treatment in lattice calculations. Gluons and quark loops which are not directly connected to the photons, which will be automatically included in dynamical lattice calculations, are not shown.

The function $\mathscr{M}$ include the muon propagators and the three internal photon propagators. These muon and photon propagators are simply the free fermion and photon propagators, whose analytical form is known. Therefore one can either calculate $\mathscr{M}$ on a finite volume lattice [16, 17,

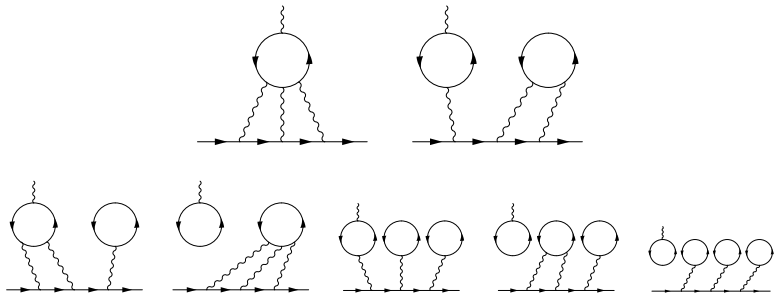

Figure 3: HLbL diagrams in lattice calculation. For each of the above diagrams, there are other possible permutations of the connections between the three internal photons and the muon line that are not shown. The first row shows the only two type of diagrams which do not vanish in the flavor SU(3) limit.

18], or semi-analytically in infinite volume [19, 20, 21, 22]. We will refer to $\mathscr{M}$ as the weighting function or the QED kernel.

Apart from using lattice QCD to calculate HLbL directly, the lattice can also be used to obtain other useful information related to HLbL. In Ref [23], the hadronic 4-point function is studied in many different channels and compared with model and dispersive sum rules. In Ref [24], the pion-pole contribution to HLbL, which is one of the most important channels in the dispersive analysis, is studied. In Ref [25, 26], some attempt to formulate the pion-pole contribution in coordinate space, which can be used to compare with the direct lattice calculation is made.

In this contribution, I will report on recent progress in the direct calculation of the HLbL contribution on the lattice. The status of the calculations of the HVP contribution is covered by the talk given by Kohtaroh Miura [27] and Marina Marinkovic [28].

2. Evaluate with the $\mathrm{QED_L}$ formulation

2.1 Subtraction method

The first lattice calculation of HLbL is performed by the RBC-UKQCD collaboration [16]. A carefully designed subtraction scheme [29] is used to reduce the rather complicated HLbL diagram to the difference of two much simpler diagrams, as shown in Fig. 4. The quark loop of the simpler diagram is evaluated using the point source propagator, whose source is located at the vertex connecting to the external photon. One of the three internal photon propagators, which is drawn in the diagram, connecting the quark loop and the muon line, is explicitly included. Two vertices connected by this photon propagator are summed over the entire lattice exactly. The other two internal photon propagators in the diagrams emerge from computing the quark and muon propagators within the quenched $U(1)$ (QED) gauge configurations. Different from the QCD gauge configurations, the QED gauge configurations are generated with Feynman gauge, and with the $\mathrm{QED_L}$ prescription [30], where all spatial zero modes are removed to cure the infrared singularity. In order to extract the form factor $F_2(q^2)$ relevant to $g-2$, whose effect is proportion to q, a non-zero momentum transfer q is used in the calculation. On a lattice with a finite volume, q is chosen to be multiples of $2\pi/L$. Since $a_\mu = F_2(q^2=0)$, extrapolation to $q=0$ is needed.

The proof of concept calculation is performed using this method with an RBC-UKQCD collaboration 2+1 flavor, DWF+Iwasaki ensemble [31, 32]. The lattices are of size $24^3 \times 64$, with

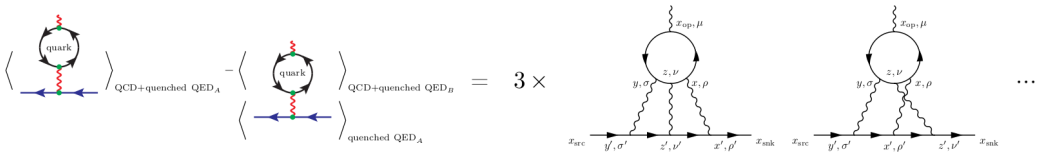

Figure 4: Illustration of the subtraction method.

pion mass equals to $m_\pi = 340$MeV and inverse lattice spacing equals $a^{-1} = 1.78$GeV. The size of the lattice is $L = 2.66$fm. An unphysical muon mass $m_\mu = 178$MeV was chosen in the calculation ($m_\mu a = 0.1$). The results of the calculation are shown in Fig. 5 as black diamonds. The calculation is performed for multiple muon source-sink separations, the x-axis of the plot. As the first, exploratory, lattice QCD calculation of HLbL, this result is promising and suggest the feasibility of a more precise calculation with physical mass and larger volumes.

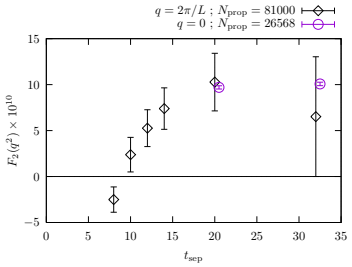

Figure 5: Comparison between the subtraction method (black diamonds) [16] and the point source method (purple circles) [17]. The x-axis is the time separation between the source and sink for the muon, which should be large enough to capture all the contributions. The two calculations are consistent within errors, and the point source method is more accurate with less cost - the number of quark propagators calculated, $N_{\rm prop}$, is shown in the legend of the plot.

2.2 Moment method

A series of improvements are made on top of the initial subtraction method by RBC-UKQCD collaboration [17]. Most of the improvements aimed at reducing the statistical error. The use of the stochastic QED gauge field, which was the major source of the statistical error, is completely eliminated. Instead, the new method evaluates the hadronic four-point function with two stochastically sampled two point sources, and all the photon propagators are evaluated exactly, using Feynman gauge and the QED$_{\rm L}$ prescription. Fig. 6 illustrate the location of the point sources. Apart from the two point sources, all the other vertices can be completely summed over the entire lattice, and all the propagators are exactly calculated on a given QCD configuration. This is a significant improvement in reducing the statistical error compare with the previous subtraction method.

Apart from the stochastically generated QCD gauge ensemble, the sampling of the point pair x and y is the only stochastic procedure in the calculation. To increase the efficiency of the sampling, importance sampling is employed. Since most contribution comes from the short distance region where x and y are close, and the long-distance region are suppressed exponentially by some hadron mass scale times the distance, the short-distance point pairs are sampled more often than the long-distance ones. Especially, we perform a complete sampling up to discrete symmetry for distances less or equal to $r_{\rm max}$, which is usually chosen to be 5 lattice spacing.

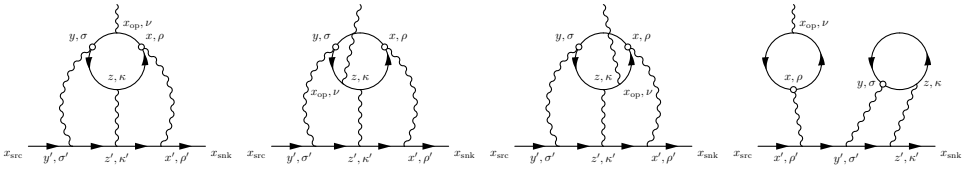

Figure 6: Moment method for the connected diagrams (first three) and the leading disconnected diagrams (last one). Point sources are represented by small circles at x and y. Permutations of the photon vertices on the muon line are not drawn but are included in calculations.

Another improvement with the moment method is that: we can avoid the difficulty of taking $q \to 0$ through extrapolation, which is necessary for the subtraction method, by directly calculating $F_2(q^2)$ at the point of interest $q^2 = 0$. The formula is similar to the classical formula to calculate the magnetic moment, Eq (2.1). The precise connection is worked out in Ref. [17].

$$\vec{\mu} = \frac{1}{2}\int d^3 r[\vec{r} \times \vec{J}(\vec{r})]. \tag{2.1}$$

With the moment method, we repeat the $24^3 \times 64$, $m_\pi = 340$MeV, connected diagrams calculation, and compare with the subtraction method. The result is shown in Fig. 5, and consistent with the previous method. The statistical errors are significantly reduced, despite the smaller computational cost and directly computing at the $q = 0$ point. Thanks to the exact photon propagators, the error does not increase with the increase of the source and sink separation of the muon line, so $t_{\text{sep}} = T/2$ is used in all the following calculation.

The moment method also applies to the leading disconnected diagrams in Fig. 6. It is also shown that the vacuum expectation value of individual loops should be subtracted before calculating the product of the two loops, not because the vacuum subtraction is needed to ensure gluon exchanges between the two loops, but because of the statistical error reduction result from this subtraction.

Another trick to reduce the statistical error for the disconnected diagrams is the M^2 trick. One can sample M points on each configuration and calculate point source propagators for each sampled points. Then, any pair of point source propagators from the same configuration can be combined to calculate the disconnected diagram in Fig. 6. Overall, this corresponds to $M(M-1)/2$ combinations per configuration. Typically, M is on the order of a thousand, and this trick significantly enhances the statistics.

2.3 Lattice results from the 48I ensemble

RBC-UKQCD collaboration applied the moment method to the 48I, 2+1 flavor, DWF+Iwasaki ensemble, where $m_\pi = 139$MeV, $a = 0.113$fm, and $L = 5.47$fm [33]. The calculation is performed for the connected diagrams and the leading disconnected diagrams [18]:

$$a_\mu^{\text{con,48I}} = (11.60 \pm 0.96) \times 10^{-10}, \tag{2.2}$$

$$a_\mu^{\text{discon,48I}} = (-6.25 \pm 0.80) \times 10^{-10}, \tag{2.3}$$

$$a_\mu^{\text{total,48I}} = (5.35 \pm 1.35) \times 10^{-10}. \tag{2.4}$$

The fact that the leading disconnected diagram contribution is significant and negative is not a surprise. This can be explained by how the π^0 pole contribution is distributed to the connected

diagrams and the leading disconnected diagrams [34, 35]. It should be noted the above results is obtained with only one lattice spacing and volume. The errors quoted above are statistical only, and the discretization error or the finite volume error, which can be very significant, are not included.

In addition to the fully integrated results above obtained with Eqs. (**??**)(**??**), the way the integration is performed also gives partial integral up to an arbitrary upper limit for r, the separation between the two point-source locations x and y. Because of the symmetry between the three points x, y, and z, the summation over z is arranged so that the separation between x and y is smaller than $|x-z|$ and $|y-z|$. The partial integral as a function of the upper limit of r is plotted in Fig. 7.

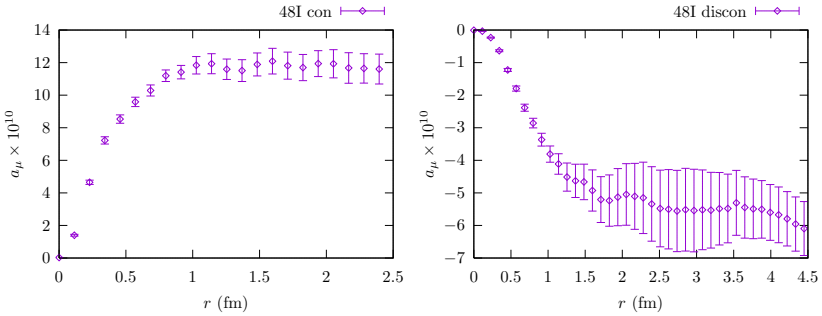

Figure 7: Left: connected diagram. Right: disconnected diagrams. For both plots, r is the upper limit on $|x-y|$, and the curve corresponds to the partial integral given the upper limit on $|x-y|$. Results are obtained by RBC-UKQCD collaboration with the 48I ensemble, where $m_\pi = 139$MeV, $a = 0.113$fm, and $L = 5.47$fm [33, 18].

2.4 Continuum limit from the 64I ensemble

RBC-UKQCD starts by studying the discretization error by repeat the calculation on a finer ensemble, the 64I ensemble, where $m_\pi = 139$MeV, $a = 0.083$fm, and $L = 5.34$fm [33]. The HLbL calculation was performed with slightly partial quenched pion mass $m_\pi = 135$MeV. In order to take the continuum limit, a small portion (5 configurations) of the 48I ensemble is recomputed also with the partially quenched pion mass $m_\pi = 135$MeV, in a correlated fashion, the small correction is then added to the unitary 48I results above. Because domain wall fermion was used in the calculation, the discretization errors are expected to be proportion to a^2. The following formula is then used to extrapolate to the continuum limit:

$$a_\mu(a,L) = a_\mu(0,L)(1-c_1 a^2), \tag{2.5}$$

where $a_\mu(a,L)$ is HLbL evaluated with non-zero lattice spacing a and finite volume L, and $a_\mu = a_\mu(0,\infty)$. The results obtained from 48I, 64I, extrapolation with Eq. (2.5) is plotted in Fig. 8.

The extrapolated continuum results are

$$a_\mu^{\text{con,48I-64I}} = (16.94 \pm 3.77) \times 10^{-10}, \tag{2.6}$$

$$a_\mu^{\text{discon,48I-64I}} = (-12.31 \pm 3.39) \times 10^{-10}, \tag{2.7}$$

$$a_\mu^{\text{total,48I-64I}} = (4.63 \pm 4.44) \times 10^{-10}. \tag{2.8}$$

The statistical error from the continuum limit is very large, especially after the cancelation between the connected diagrams and the disconnected diagrams. The enhancement of the statistical error overwhelms the reduction of possible discretization error. In order to benefit from the results from

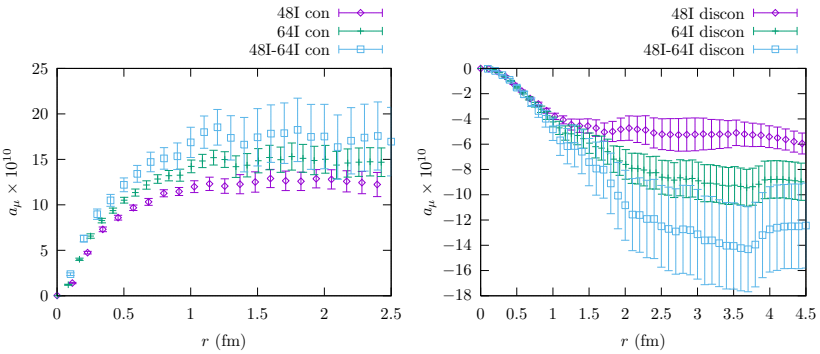

Figure 8: Left: connected diagram. Right: disconnected diagrams. For both plots, r is the upper limit on $|x-y|$, and the curve corresponds to the partial integral given the upper limit on $|x-y|$. Results are obtained by RBC-UKQCD collaboration with the 48I ensemble, 64I ensemble, and extrapolation with Eq. (2.5) [33, 18].

the 64I calculation, the HLbL contribution is split into two parts, and treat them separately:

$$a_\mu = a_\mu^{\text{short}} + a_\mu^{\text{long}} \tag{2.9}$$

where $a_\mu^{\text{short}} = a_\mu^{\text{short}}(r_s) = a_\mu(r \leqslant r_s)$, $a_\mu^{\text{long}} = a_\mu^{\text{long}}(r_s) = a_\mu(r > r_s)$, and $r_s = 1.0$fm. With these definitions, Fig. 7 and Fig. 8 can be viewed as plotting the a_μ^{short} as a function of r_s. From the plots, it can be seen that a_μ^{short} captures most of the contribution and has a relatively small statistical error. The continuum limit is calculated with extrapolation using Eq. (2.5):

$$a_\mu^{\text{short,48I-64I}} = a_\mu^{\text{short,extrap-48I-64I}}. \tag{2.10}$$

The long distance part, a_μ^{long}, on the other hand, is much noisier but the contribution is relatively insignificant. As a trade-off between systematic error and statistical error, it is beneficial to not use extrapolation, but use the results from the 48I ensemble directly. The $\mathcal{O}(a^2)$ systematic error of the 48I result is estimated according to the short distance part of the connected diagram, where extrapolation can be performed accurately.

$$a_\mu^{\text{long,48I-64I}} = a_\mu^{\text{long,48I}} \left(1 \pm \left| \frac{a_\mu^{\text{con,short}}}{a_\mu^{\text{con,short,48I}}} - 1 \right| \right). \tag{2.11}$$

The above estimation of the $\mathcal{O}(a^2)$ systematic error is rather conservative, since the relative discretization error for the short distance is expected to be larger than the long-distance part. With this hybrid strategy of taking the continuum limit, the following results are obtained:

$$a_\mu^{\text{con,48I-64I}} = (17.35 \pm 1.97 \pm 0.20_{\text{sys},a^2}) \times 10^{-10}, \tag{2.12}$$

$$a_\mu^{\text{discon,48I-64I}} = (-7.26 \pm 1.11 \pm 1.02_{\text{sys},a^2}) \times 10^{-10}, \tag{2.13}$$

$$a_\mu^{\text{total,48I-64I}} = (10.09 \pm 1.90 \pm 1.22_{\text{sys},a^2}) \times 10^{-10}. \tag{2.14}$$

The statistical errors are all calculated with the jackknife method, and correlations between the connected and disconnected results are taken into account. The $\mathcal{O}(a^2)$ systematic error for the total is estimated by adding the systematic error of the connected and disconnected diagrams. Comparing with plain continuum limit result in Eq. (2.8), the above results with the hybrid continuum limit are consistent with the old results, but much more accurate.

2.5 Infinite volume limit

Finite volume calculations involving the photons and use the QED_L formulation usually have power-law like finite volume errors. In the case of the calculation of QED self-energy diagram for massive charged particles, the finite volume error using QED_L is $\mathcal{O}(1/L)$ [30]. In the case of HLbL, because the internal photons are emitted from a quark loop instead of a quark line, the finite volume effects are smaller than the case of QED self-energy diagram. It can be shown that the finite volume effects are $\mathcal{O}(1/L^2)$ [17]. Therefore, one can use the following equation to extrapolate to the infinite volume limit.

$$a_\mu(a,L) = a_\mu(a,\infty)\left(1-\frac{c_2}{(m_\mu L)^2}\right) = a_\mu(1-c_1a^2)\left(1-\frac{c_2}{(m_\mu L)^2}\right) \tag{2.15}$$

The fitting formula can be tested in a simpler muonic LbL calculation, where the quark loop is replaced by a muon loop. Numerically, the same lattice method is used in the test calculation. All the propagators are still calculated on a lattice with finite lattice spacing and volume. The only difference between this test and a full QCD calculation is that no QCD configurations are used in the test. Three physical lattice sizes: 6.0fm, 9.0fm, 12.0fm are used in the test muonic LbL calculation, each with three lattice spacings. The results are plotted in Fig. 9 on the left. The curves are the results of the fit using Eq. (2.15) and only three data points in the lower right corner – relatively small volume and coarse lattices that mimics the QCD calculations. The extrapolated results are off by 13%.

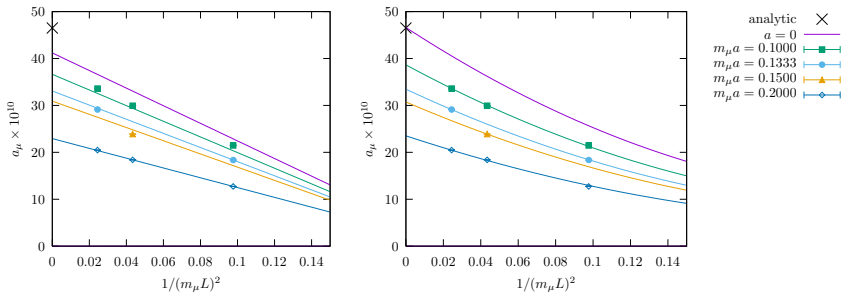

Figure 9: Left: fit with Eq. (2.15) and only using the three data points from relatively small volume and coarse lattices: $m_\mu a = 0.2$ $L/a = 16$; $m_\mu a = 0.2$ $L/a = 24$; $m_\mu a = 0.1333$ $L/a = 24$. The extrapolated result is $a_\mu^{\text{muonic-LbL}} = 41.19(6)\times 10^{-10}$. Right: fit with Eq. (2.16) using all the data points. The extrapolated result is $a_\mu^{\text{muonic-LbL}} = 46.61(19)\times 10^{-10}$. The errors are all statistical. The data points are from Ref. [17] by RBC-UKQCD collaboration. The extrapolated result is to be compared with the analytic result $a_\mu^{\text{muonic-LbL}} = 0.371\times(\alpha_{\text{QED}}/\pi)^3 = 46.50\times 10^{-10}$ [36].

To fully profit from the 9 data points, higher order effects can be included in the fit. The following equation describes all the data points very well and the extrapolated value $46.61(19)\times 10^{-10}$ agree very well with the analytic result 46.50×10^{-10} obtained with the continuum and infinite volume calculation [36].

$$a_\mu(a,L) = a_\mu(1-c_1a^2+c_1'a^4)\left(1-\frac{c_2}{(m_\mu L)^2}+\frac{c_2'}{(m_\mu L)^4}\right) \tag{2.16}$$

Following the successful muonic LbL test strategy, RBC-UKQCD collaboration has performed HLbL on several DWF+DSDR ensembles with different lattice sizes, ranges from 4.8fm to 9.6fm [37]. The results are plotted in Fig. 10 and extrapolated to continuum limit and infinite volume

with Eq. (2.15):

$$a_\mu^{\text{con}} = (26.12 \pm 3.87 \pm 0.28_{\text{sys},a^2}) \times 10^{-10}, \tag{2.17}$$

$$a_\mu^{\text{discon}} = (-12.87 \pm 2.27 \pm 1.63_{\text{sys},a^2}) \times 10^{-10}, \tag{2.18}$$

$$a_\mu^{\text{total}} = (13.24 \pm 4.40 \pm 1.91_{\text{sys},a^2}) \times 10^{-10}. \tag{2.19}$$

The remaining systematics to be estimated are the missing subleading diagrams and the $\mathscr{O}(a^4)$ or $\mathscr{O}(1/L^4)$ effects. In the case of the muonic LbL these effects are 13% even with quite coarse lattice spacings and modest lattice volumes.

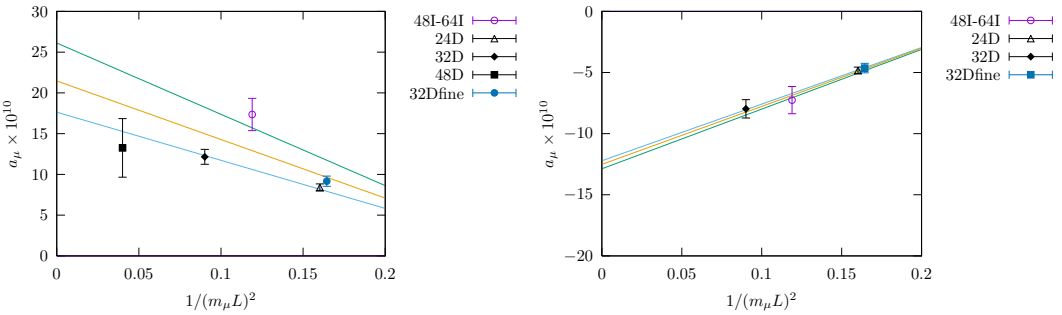

Figure 10: Infinite volume extrapolation from RBC-UKQCD. Left: connected diagrams. Right: disconnected diagrams.

3. Evaluate with the QED$_\infty$ formulation

3.1 Mainz approach

Mainz group has developed a strategy to calculate HLbL on lattice independently from RBC-UKQCD [19, 20, 22]. Harvey Meyer had the initial idea after the Muon $g-2$ workshop at Mainz in April 2014. The Mainz strategy is also formulated in coordinate space and make heavy use of point source propagators, which is similar to the RBC-UKQCD's approach. However, the Mainz approach carries a significant new feature. The Mainz group invented a method to evaluate the QED kernel $\mathscr{M}$ semi-analytically in the infinite volume and continuum limit. This function can be pre-computed on a grid, saved to disk, once and for all. This method will completely eliminate the $\mathscr{O}(1/L^2)$ finite volume effects in the previous QED$_\text{L}$ calculations.

When evaluating the infinite volume QED kernel, the Mainz group has averaged over the muon propagation direction, leading to a manifestly Lorentz covariant QED kernel, with only three parameters. Since the QED kernel is evaluated in Euclidean space, Lorentz covariance is actually 4D rotational covariance. The 4-D summation of the $y-z$ reduced to 1-D integral of $|y-z|$. This idea can also be applied to the lattice HVP calculations [38].

The hadronic four-point function $\mathscr{H}$ (at least the connected contribution) is evaluated with two point sources at x and y. Because of the Lorentz covariant formulation of the QED kernel, Mainz always chooses the $y-x$ to be of the form (i,i,i,i) in order to reduce the finite volume and discretization effects.

The infinite QED kernel is successfully tested in two cases, whose results are known in momentum space calculations [39]. Results are plotted in Fig. 11.

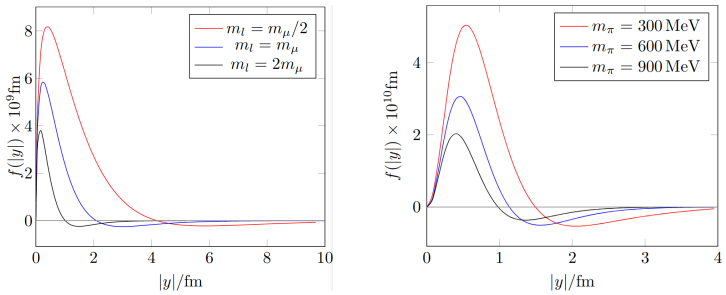

Figure 11: After performing the integration for $|y|$, the results agree with analytic results obtained in momentum space, suggests that the QED kernel $\mathscr{M}$ is successful [39]. Left: leptonic LbL with different lepton masses. Right: pion-pole contribution to LbL with the VMD model for the pion transition form factor.

3.2 RBC-UKQCD approach

Motivated by Mainz's success, RBC-UKQCD also starts the QED_∞ kernel project by evaluating the weighting function, $\mathscr{M}$, in infinite volume limit and using continuum propagator formula [21]. Different from the Mainz's covariant formulation, the time direction of the lattice is set to be the muon propagating direction of the LbL diagram, the same as the QED_L case. As the infinite volume formalism being developed, RBC-UKQCD noticed that a class of subtractions can be performed for $\mathscr{M}$ without affecting the final HLbL results because of the consequence of the current conservation property satisfied by the hadronic 4-point function:

$$\int d^4x \mathscr{H}(x,y,z,x_{\text{op}}) = 0 \qquad \text{(in infinite volume and in continuum)} \tag{3.1}$$

The following subtraction scheme is designed to reduce the magnitude of the $\mathscr{M}$, especially when two of the vertices are close. It is expected that the statistical error and the discretization error Find a way to reduce discretization effects and finite volume effects:

$$\mathscr{M}^{(\text{sub})}(x,y,z) = \mathscr{M}(x,y,z) - \mathscr{M}(y,y,z) - \mathscr{M}(x,y,y) \tag{3.2}$$

The subtraction terms' final vanishes in infinite volume and continuum limit. At non-zero lattice spacing or finite volume: proper choice of subtraction term can reduce the two systematics.

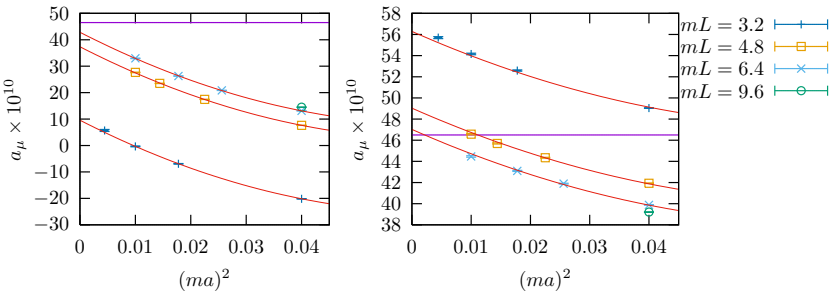

Figure 12: Continuum extrapolation for muon leptonic light-by-light. Left: original QED kernel. Right: subtracted QED kernel. Note the vertical scales of the two plots are different. Discretization error and finite volume error are greatly reduced for the subtracted kernel.

The subtraction on the QED kernel also proves helpful in Mainz's QED_∞ formulation [40, 41]. Note that the Mainz group tried a few subtraction methods, the one used in QCD simulations is the

following:

$$\mathscr{M}^{(2)}(x,y,z) = \mathscr{M}(x,y,z) - \mathscr{M}(z,y,z) - \mathscr{M}(x,z,z) \tag{3.3}$$

which is different from the RBC-UKQCD subtraction formula Eq. (3.2).

3.3 Check between Mainz and RBC-UKQCD

Before we can obtain the HLbL contribution at physical pion mass and control all the systematics, it is possible to perform cross-check between the Mainz and RBC-UKQCD at some heavier than physical pion mass for the connected diagram. Due to the difference in the choice of the time direction, the subtraction scheme of the QED kernel, the point source location sampling strategy, treatment of the boundary, and the lattice action, the results from the two groups do not need to agree unless in the infinite volume and continuum limit. During the "Second Plenary Workshop of the Muon g-2 Theory Initiative" workshop at Mainz, it is agreed that the check shall be performed at $m_\pi = 340$MeV for the connected diagrams, in the infinite volume and continuum limit.

3.3.1 Mainz

Three different pion masses, m_π: 200MeV, 285MeV, 340MeV, are used to study the pion mass dependence. The calculations are performed at the fixed lattice spacing ($a = 0.064$fm) and the fixed volume ($L = 3.1$fm). Finite volume effects are studied with two different volumes, L: 2.75fm, 4.13fm, with $m_\pi = 285$MeV and $a = 0.086$fm. Discretization effects are studied with two different a: 0.086fm, 0.064fm, with fixed $m_\pi = 285$MeV and two similar volumes $L = 2.7\text{fm}, 3.1\text{fm}$, respectively.

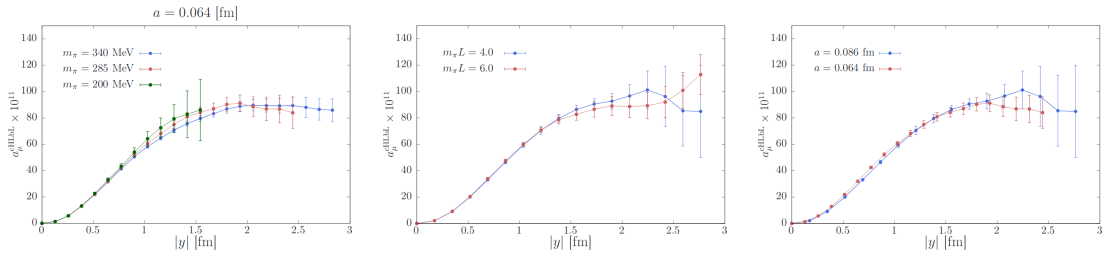

Pion mass dependence | Finite volume effects | Discretization effects

Figure 13: Mainz preliminary results, the variable $|y|$ is the separation between the two point sources [40].

From the above studies, it is obtained that $a_\mu^{\text{cHLbL}} = 8.2(9) \times 10^{-10}$ at $m_\pi = 340$MeV, $L = 3.1$fm, $a = 0.064$fm [40]. Mainz group is still accumulating statistics, and the statistical error is expected to be reduced in the future. Finite volume effects and discretization effects are found to be small based on the study with $m_\pi = 285$MeV.

3.3.2 RBC-UKQCD

RBC-UKQCD's results are plotted in Fig. 14. It can be seen that the physical pion mass result is significantly different from the results of the two heavier pion mass. There is a sizable difference between these two volumes. Further study is required to extrapolate to the infinite volume limit.

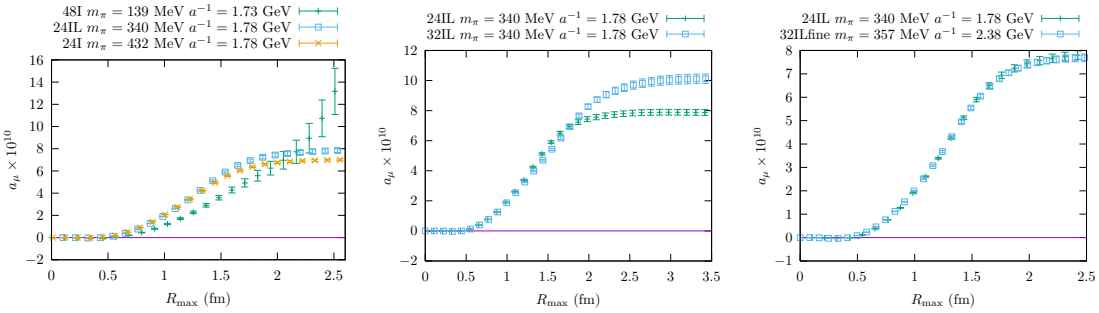

Pion mass dependence | Finite volume effects | Discretization effects

Figure 14: RBC-UKQCD's preliminary results. Connected contribution calculated with subtracted QED$_\infty$ kernel plotted as partial sum on $R_{\max} = \max\{|x-y|, |y-z|, |z-x|\}$. Most results are obtained with heavier than physical pion mass ensembles [31, 32].

3.4 Combine with pion pole contribution using $\pi^0 \to \gamma\gamma$ form factor

While the power-law finite volume effects are completely eliminated with the QED$_\infty$ method, the finite volume effect from the QCD part can still be sizable despite being suppressed exponentially. Based on the pion-pole model calculation in coordinate space [42, 26], rather large lattice size, $\sim$ 10fm, is needed to control the finite volume effects from the pion-pole contribution. As pion being the lightest particle in QCD, the large finite volume effect is not entirely unexpected. Making the situation worse, the statistical error for large distance region is hard to control with the QED$_\infty$ weighting function, even after subtraction is performed. However, if one split the contribution of the HLbL into the short distance part and the long distance part based on the separation between the vertices locations, e.g. $R_{\max} = \max\{|x-y|, |y-z|, |z-x|\}$. The short distance part can be obtained by direct lattice calculation. The long distance part can be approximated by pion-pole contribution.

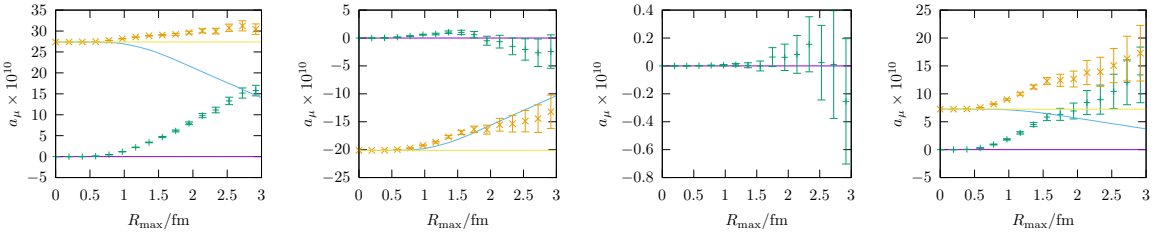

con | leading discon | first subleading discon | total

Figure 15: RBC-UKQCD preliminary results using the 24D ensemble [37] and the subtracted QED$_\infty$ weighting function [21]. The x-axis is $R_{\max} = \max\{|x-y|, |y-z|, |z-x|\}$. The green "+" is the lattice data plotted as partial sum up to $R_{\max}$. The light yellow line is the LMD model's pion-pole total results, and the blue curve is the LMD model's pion-pole contribution in coordinate space plotted as a reverse partial sum [26]. The pion-pole contribution can be attributed to specific diagrams by multiplying corresponding factors [34, 35, 23]. The orange "×" is the combination of lattice results in the shorter distance region and LMD model pion-pole results in the longer distance region.

Fig. 15 plots the RBC-UKQCD's preliminary results with subtracted QED$_\infty$ and physical pion mass for the connected diagram, leading disconnected diagrams, and the first subleading disconnected diagrams (shown in the second row of Fig. 3). The lattice calculation is performed with the 24D ensemble [37] with $a = 0.2$fm and $L = 4.8$fm. The combined results from lattice and LMD

model, at the switch point $R_{\text{max}} = 2.0$fm, is

$$a_\mu^{\text{con}} = (29.62 \pm 0.33) \times 10^{-10}, \tag{3.4}$$

$$a_\mu^{\text{discon}} = (-16.42 \pm 0.81) \times 10^{-10}, \tag{3.5}$$

$$a_\mu^{\text{first subleading discon}} = (0.06 \pm 0.10) \times 10^{-10}, \tag{3.6}$$

$$a_\mu^{\text{total}} = (13.26 \pm 0.88) \times 10^{-10}. \tag{3.7}$$

The errors are statistical only. There are many systematic effects remain to be estimated and improved. In particular, the long distance part shall be replaced by data-driven results to reduce LMD model uncertainty, the larger lattice ensemble and larger R_{max} shall be used to reduce the finite volume error for the short distance part and to increase the accuracy of the pion-pole approximation of the long distance part.

4. Summary and outlook

Lots of progress on conceptual and technical side achieved for HLbL on the lattice in the last 3-4 years by Mainz and RBC-UKQCD. The RBC-UKQCD collaboration obtained many results at physical pion mass with QED_L for the fully connected and leading disconnected diagrams. Progress is also made using the infinite volume QED kernel method and the subleading disconnected diagrams. The Mainz group pioneered the semi-analytical approach for QED kernel in the continuum and infinite volume to have full control over non-QCD part of HLbL. Results for QCD connected diagram contribution at several pion masses (lattice spacings, and volumes) are obtained. During the "Second Plenary Workshop of the Muon g-2 Theory Initiative" workshop, it is planned that a cross-check shall be performed at $m_\pi = 340$MeV between Mainz and RBC-UKQCD using the QED_∞ method. More work on the cross check is needed.

The final goal is to obtain a consolidated number with 10% uncertainty and controlled systematics by both RBC-UKQCD and Mainz before the time the Fermilab experiment publishes its final result – 2-3 years later from now. The progress made so far make this goal quite promising. There was a claim that muon $g-2$ is not a very useful quantity to probe new physics, because one can never control the uncertainty of HLbL. Now, we know we will be able to nail it down.

Acknowledgments

I thank the following for willingly sharing their results and discussing their work: N. Asmussen, T. Blum, N. Christ, A. Gerardin, M. Hayakawa, T. Izubuchi, C. Jung, C. Lehner, H. B. Meyer, A. Nyffeler.

References

[1] J. S. Schwinger. In: *Phys. Rev.* 73 (1948), pp. 416–417.

[2] G. Bennett et al. In: *Phys.Rev.* D73 (2006), p. 072003. arXiv: hep-ex/0602035 [hep-ex].

[3] R. M. Carey et al. In: (2009).

[4] T. Mibe. In: *Chin. Phys.* C34 (2010), pp. 745–748.

[5] T. Aoyama et al. In: *Phys.Rev.Lett.* 109 (2012), p. 111808. arXiv: 1205.5370 [hep-ph].

[6] C. Gnendiger, D. Stockinger, and H. Stockinger-Kim. In: *Phys.Rev.* D88 (2013), p. 053005. arXiv: 1306.5546 [hep-ph].

[7] T. Blum et al. In: *Phys. Rev. Lett.* 121.2 (2018), p. 022003. arXiv: 1801.07224 [hep-lat].

[8] F. Jegerlehner. In: *EPJ Web Conf.* 166 (2018), p. 00022. arXiv: 1705.00263 [hep-ph].

[9] J. Prades, E. de Rafael, and A. Vainshtein. In: *Adv. Ser. Direct. High Energy Phys.* 20 (2009), pp. 303–317. arXiv: 0901.0306 [hep-ph].

[10] K. T. Engel, H. H. Patel, and M. J. Ramsey-Musolf. In: *Phys. Rev.* D86 (2012), p. 037502. arXiv: 1201.0809 [hep-ph].

[11] G. Colangelo et al. In: *JHEP* 09 (2014), p. 091. arXiv: 1402.7081 [hep-ph].

[12] M. Hoferichter et al. In: *JHEP* 10 (2018), p. 141. arXiv: 1808.04823 [hep-ph].

[13] G. Colangelo et al. In: *Phys. Rev. Lett.* 118.23 (2017), p. 232001. arXiv: 1701.06554 [hep-ph].

[14] G. Colangelo et al. In: *JHEP* 04 (2017), p. 161. arXiv: 1702.07347 [hep-ph].

[15] G. Colangelo et al. In: *EPJ Web Conf.* 175 (2018), p. 01025. arXiv: 1711.00281 [hep-ph].

[16] T. Blum et al. In: *Phys.Rev.Lett.* 114.1 (2015), p. 012001. arXiv: 1407.2923 [hep-lat].

[17] T. Blum et al. In: *Phys. Rev.* D93.1 (2016), p. 014503. arXiv: 1510.07100 [hep-lat].

[18] T. Blum et al. In: *Phys. Rev. Lett.* 118.2 (2017), p. 022005. arXiv: 1610.04603 [hep-lat].

[19] J. Green et al. In: *PoS* LATTICE2015 (2016), p. 109. arXiv: 1510.08384 [hep-lat].

[20] N. Asmussen et al. In: *PoS* LATTICE2016 (2016), p. 164. arXiv: 1609.08454 [hep-lat].

[21] T. Blum et al. In: *Phys. Rev.* D96.3 (2017), p. 034515. arXiv: 1705.01067 [hep-lat].

[22] N. Asmussen et al. In: *EPJ Web Conf.* 175 (2018), p. 06023. arXiv: 1711.02466 [hep-lat].

[23] A. Gérardin et al. In: *Phys. Rev.* D98.7 (2018), p. 074501. arXiv: 1712.00421 [hep-lat].

[24] A. Gérardin, H. B. Meyer, and A. Nyffeler. In: *Phys. Rev.* D94.7 (2016), p. 074507. arXiv: 1607.08174 [hep-lat].

[25] C. Tu. In: *Proceedings, The 36th Annual International Symposium on Lattice Field Theory (LATTICE2018)*. 2018.

[26] L. Jin. In: *Second Plenary Workshop of the Muon g-2 Theory Initiative*. 2018.

[27] K. Miura. In: *Proceedings, The 36th Annual International Symposium on Lattice Field Theory (LATTICE2018)*. 2018.

[28] M. Marinkovic. In: *Proceedings, The 36th Annual International Symposium on Lattice Field Theory (LATTICE2018)*. 2018.

[29] M. Hayakawa et al. In: *PoS* LAT2005 (2006), p. 353. arXiv: hep-lat/0509016 [hep-lat].

[30] M. Hayakawa and S. Uno. In: *Prog. Theor. Phys.* 120 (2008), pp. 413–441. arXiv: 0804.2044 [hep-ph].

[31] C. Allton et al. In: *Phys.Rev.* D78 (2008), p. 114509. arXiv: 0804.0473 [hep-lat].

[32] Y. Aoki et al. In: *Phys.Rev.* D83 (2011), p. 074508. arXiv: 1011.0892 [hep-lat].

[33] T. Blum et al. In: *Phys. Rev.* D93.7 (2016), p. 074505. arXiv: 1411.7017 [hep-lat].

[34] J. Bijnens and J. Relefors. In: *JHEP* 09 (2016), p. 113. arXiv: 1608.01454 [hep-ph].

[35] L. Jin et al. In: *PoS* LATTICE2016 (2016), p. 181. arXiv: 1611.08685 [hep-lat].

[36] S. Laporta and E. Remiddi. In: *Phys. Lett.* B265 (1991), pp. 182–184.

[37] R. Mawhinney. In: *Proceedings, The 36th Annual International Symposium on Lattice Field Theory (LATTICE2018)*. 2018.

[38] H. B. Meyer. In: *Eur. Phys. J.* C77.9 (2017), p. 616. arXiv: 1706.01139 [hep-lat].

[39] N. Asmussen et al. In: *EPJ Web Conf.* 179 (2018), p. 01017. arXiv: 1801.04238 [hep-lat].

[40] N. Asmussen. In: *Second Plenary Workshop of the Muon g-2 Theory Initiative*. 2018.

[41] N. Asmussen et al. In: *15th International Workshop on Tau Lepton Physics (TAU2018) Amsterdam, Netherlands, September 24-28, 2018*. 2018. arXiv: 1811.08320 [hep-lat].

[42] A. Nyffeler. In: *Second Plenary Workshop of the Muon g-2 Theory Initiative*. 2018.